室蘭工業大学
学術資源アーカイブ
Muroran Institute of Technology Academic Resources Archive

Effect of Co Doping on the Structure and Magnetic Properties of TmMn1-xCoxO3

メタデータ	言語: English 出版者: The Physical Society of Japan 公開日: 2019-07-01 キーワード (Ja): キーワード (En): 作成者: 坂爪, 康則, バオ, ジンファ, 大杉, 駿介, 雨海, 有佑, 高野, 英明 メールアドレス: 所属:
URL	http://hdl.handle.net/10258/00009943

Effect of Co Doping on the Structure and Magnetic Properties of $TmMn_{1-x}Co_xO_3$

Yasunori Sakatsume, JianHua Bao, Shunsuke Ohsugi,
Yusuke Amakai, and Hideaki Takano*

Graduate School of Engineering, Muroran Institute of Technology,
27-1 Mizumoto-cho, Muroran, Hokkaido 050-8585, Japan

(Received)

We report the structure and magnetic properties of Co-doped $TmMnO_3$ polycrystals for Co doping levels of $0 \leq x \leq 0.9$. $TmMnO_3$ (x=0) prepared at ambient pressure was hexagonal. Hexagonal and orthorhombic phases coexisted in $TmMn_{1-x}Co_xO_3$ for $0 \leq x < 0.5$. We obtained almost single-phase orthorhombic samples with $0.5 \leq x \leq 0.9$ using complex polymerization. Ferromagnetic orthorhombic $TmMn_{1-x}Co_xO_3$ formed upon Co doping. The ionic states of Tm, Mn, and Co were determined through magnetization measurements. The rapid decrease in magnetization for $0.5 \leq x \leq 0.7$ below about 25 K was explained using a model consisting of a combination of ferromagnetic Mn-Co and paramagnetic Tm sublattices.

*E-mail: takano@mmm.muroran-it.ac.jp

1. Introduction

The manganese rare-earth oxide $RMnO_3$ has been investigated extensively because of its diverse physical properties and potential applications.[1-4] Moreover, detailed studies on R-site and Mn-site substitutions have been carried out.[5-8] Upon the substitution of R with divalent elements such as Sr and Ca, and of Mn with other transition metals such as Co, Ni, and Cr, the valence of Mn partially changes from Mn^{3+} to Mn^{4+}, and the system undergoes various exchange interactions. In particular, during Co substitutions involving multiple valence states, exchange interactions among Mn^{3+}, Mn^{4+}, Co^{2+}, and Co^{3+} can be expected depending on the amount of Co substitution, and the physical properties generated by the various interactions are very interesting.

It has been reported that in hexagonal $TmMnO_3$, an antiferromagnetic spin ordering ($T_N \approx$ 82-86 K) and a ferroelectric ordering of charges (ferroelectric Curie temperature $T_{EC} \approx$ 570-593 K) may coexist.[9-11] On the other hand, $TmMnO_3$ synthesized under high pressure is orthorhombic and antiferromagnetic with a Neel temperature of 41 K and a dielectric Curie temperature of about 32 K.[12,13] The antiferromagnetic state of this system is due to the exchange interaction between Mn^{3+} ions. By realizing a mixed-valence state of Mn by replacing the Tm and/or Mn of $TmMnO_3$, it is possible to introduce a new factor into the magnetic behavior of the system. To investigate the effects of Co doping on the physical properties of $TmMnO_3$, we substituted Mn with Co and studied the structure and magnetic properties of $TmMn_{1-x}Co_xO_3$. In $TmMn_{1-x}Co_xO_3$ prepared by a solid-phase reaction, the substitution of Mn with Co induced a hexagonal-to-orthorhombic transformation for $0 \leq x \leq 0.5$, and the samples with $x \geq 0.4$ became almost single-phase orthorhombic.[14] In the Co-substituted system, the magnetization increased ferromagnetically at about 60 K with decreasing temperature, and had a maximum at around 30 K. The maximum magnetization increased with x for $0 \leq x \leq 0.5$. For $x \geq 0.5$, the amount of Tm_2O_3 impurity increased with x. The presence of this impurity made the quantitative analysis of the data difficult. In this paper, we present a new synthesis method for $TmMn_{1-x}Co_xO_3$ and describe its structure and magnetic properties.

2. Experimental Procedure

Polycrystalline $TmMn_{1-x}Co_xO_3$ ($0 \leq x \leq 0.9$) compounds were prepared by a conventional solid-state reaction (SSR) and complex polymerization (CP).[15,16] All processes were performed at ambient pressure except for the pelletization of the mixture. In the SSR method, appropriate amounts of Tm_2O_3, Mn_2O_3, and Co_3O_4, all of which were of 99.9% purity, were dried at 473 K.

These powders were ground, thoroughly mixed, and sintered at 1423 K under an O_2 atmosphere. Then, the mixtures were ground again and pelletized at 500 kgf/cm^2. These pellets were sintered at 1423 K under O_2. The starting materials used in the CP method were the metal nitrate hydrates $Tm(NO_3)_2 \cdot 4H_2O$, $Mn(NO_3)_2 \cdot 6H_2O$, and $Co(NO_3)_2 \cdot 4H_2O$, which were of 99.9% purity. These nitrates were dissolved in water and mixed with a citric acid solution. After sufficient stirring, the solution was polymerized using ethylene glycol to form a transparent polymeric gel. The temperature range for gel formation was 463 to 493 K. The gel, which was dried at 623 – 673 K on a hot plate, became a resin. This resin was easily pulverized in an agate mortar. The powder was pelletized and sintered below 1273 K under an O_2 atmosphere. The pelletization and sintering processes were repeated several times. For $x<0.5$, both the conventional SSR and CP methods were used. Quantitative differences due to sample preparation were minimal, and similar results have been reported previously.[14] For $0.5 \leq x \leq 0.9$, the CP method was used.

The crystal phases were analyzed using a MiniFlex 300 (Rigaku Co.) diffractometer with a Cu X-ray tube, a one-dimensional detector, and a Ni-Kβ filter. Structural analysis was conducted by Rietveld refinement using the software RIETAN-FP.[17] The magnetization measurements were performed with a superconducting quantum interference device (SQUID) magnetometer (Quantum Design).

3. Results and Discussion

3.1 Structure

Figure 1 shows typical X-ray diffraction (XRD) patterns for $TmMn_{1-x}Co_xO_3$ prepared by CP, with the XRD pattern for Tm_2O_3 included as a reference. $TmMnO_3$ (x=0), which was prepared at ambient pressure by the SSR, was hexagonal. These XRD patterns were refined by Rietveld analysis, and we obtained the lattice parameters a, b, c and the unit cell volume V in Fig. 2, along with the mass fraction of the hexagonal and orthorhombic phases shown in the inset, all as functions of x. The inset in Fig. 3 shows the mass fraction of the components of the SSR samples. Hexagonal and orthorhombic phases coexist for $0<x<0.5$ in samples prepared by either the SSR or CP. For $0.5 \leq x \leq 0.9$, the CP samples are almost single-phase orthorhombic, while the SSR samples contain a small amount of Tm_2O_3. The amount of this impurity in the SSR samples increases with increasing x. This indicates that the CP method is superior to the SSR method for the synthesis of samples with $0.5<x \leq 0.9$. The space group for the hexagonal phase is $P6_3cm$, and the orthorhombic phase is a distorted perovskite with the space group Pnma. The lattice parameters a_h, c_h, and V_h in the hexagonal phase are nearly constant except for the case of x=0.4.

It is considered that the discrepancies for x=0.4 are caused by errors due to the small mass fraction of the hexagonal phase. The lattice parameters a_o, b_o, c_o, and V_o for the orthorhombic phase decrease with increasing x for $0.5 \leq x \leq 0.9$. This is presumably related to the ionic radii in $TmMn_{1-x}Co_xO_3$. Peña et al. suggested that for $ErMe_xMn_{1-x}O_3$, the general formula is $RE^{3+}Mn^{4+}{}_{1-x}Co^{2+}{}_{1-x}Co^{3+}{}_{2x-1}O^{2-}{}_3$ (RE=rare-earth element) when the substitution at the manganese site exceeds 50%.[18] If we assume this valence state formula for $TmMn_{1-x}Co_xO_3$, then the average ionic radius of the 3d transition metal ions in $TmMn_{1-x}Co_xO_3$ decreases. This would qualitatively account for the decrease in the lattice parameters and the unit cell volume.

3.2 Magnetic properties

Figures 3 and 4 plot, respectively, the temperature dependences of the field-cooled (M_{FC}) and zero-field-cooled (M_{ZFC}) magnetization for the $0 \leq x \leq 0.4$ SSR samples[14] and the $0.5 \leq x \leq 0.9$ CP samples in a magnetic field of 250 Oe. The insets of Figs. 3 and 4 respectively show the mass fraction of the SSR samples and the temperature dependence of $\chi_{FC}^{-1} = H/M_{FC}$ for the CP samples above 20 K. M_{FC} increases ferromagnetically below 60 K with decreasing temperature for $0.1 \leq x \leq 0.7$. From x=0.1 to 0.5, M_{FC} increases, and then decreases from x=0.5 to 0.9. With increasing x, the mass fraction of the orthorhombic phase increases, as do M_{FC} and M_{ZFC}. A discrepancy is observed between M_{FC} and M_{ZFC} below about 160 K for $0.1 \leq x \leq 0.3$, where the hexagonal and orthorhombic phases coexist, and M_{FC} and M_{ZFC} exhibit different temperature dependences below about 60 K. M_{FC} and M_{ZFC} for $x \geq 0.5$, where the main phase is orthorhombic, are also different below about 60 K. The appearance of the orthorhombic phase induces a rapid increase in magnetization below 60 K. For x=0.8 and 0.9, there is no ferromagnetic increase, but a separation between M_{FC} and M_{ZFC} can be seen below about 60 K. We will discuss the temperature dependence of M_{FC} for the orthorhombic phase at low temperatures in more detail below.

The inverse susceptibility of $TmMn_{1-x}Co_xO_3$ ($0.5 \leq x \leq 0.9$) above 130 K, shown in the inset of Fig. 4, can be fitted as a linear function of temperature, that is, by the Curie-Weiss law:

$$\chi_{FC} = \frac{M_{FC}}{H} = \frac{C}{T-\Theta} , \quad (1)$$

where C is the Curie constant, Θ is the Weiss temperature, and H is the external magnetic field. C is related to the effective paramagnetic magnetic moment P_{eff} via

$$P_{eff}{}^2 = \frac{3Ck_B}{N\mu_B{}^2} , \quad (2)$$

where N is the number of magnetic atoms (Tm, Mn, Co) per gram, μ_B is the Bohr magneton,

and k_B is the Boltzmann constant. The values of P_{eff} and Θ, obtained from M_{FC}, are plotted in Fig. 5 as functions of x. It can be seen that Θ, which is about 15 K for x=0.5, decreases with increasing x and is negative for x≥0.8. It is found that ferromagnetic and antiferromagnetic interactions predominate for x≤0.7 and x>0.7, respectively. P_{eff} also decreases with increasing x. Ghiasi et al. investigated the valence states of Mn and Co in $LaMn_{1-x}Co_xO_3$ nanoperovskites by X-ray absorption spectroscopy.[19] They found that $LaMn_{0.75}Co_{0.25}O_3$ contained Mn^{3+}, Mn^{4+}, and Co^{2+}, while $LaMn_{0.25}Co_{0.75}O_3$ contained Mn^{4+}, Co^{2+}, and Co^{3+}, and $LaMn_{0.5}Co_{0.5}O_3$ contained Mn^{3+}, Mn^{4+}, Co^{2+}, and Co^{3+}. To facilitate the discussion, we will again assume the following valence state formula for $REMn_{1-x}Co_xO_3$ for x≥0.5: $RE^{3+}Mn^{4+}{}_{1-x}Co^{2+}{}_{1-x}Co^{3+}{}_{2x-1}O^{2-}{}_3$. Among these ions, Co^{2+} and Co^{3+} can have S=3/2 (high spin, HS) or S=1/2 (low spin, LS), and S=2 (HS) or S=0 (LS) states, respectively. Assuming that the theoretical paramagnetic moments of Tm^{3+}, Mn^{4+}, and Co^{2+} are 7.57 μ_B, 3.87 μ_B, and 3.87 μ_B (HS), respectively, at x = 0.5, P_{eff} equal to 6.01 μ_B per atom is obtained for these magnetic atoms from Eq. (3):

$$P_{eff} = \sqrt{\frac{\sum {p_i}^2}{2}} \ . \qquad (3)$$

The 2 in the dominator of Eq. (3) corresponds to the number of magnetic atoms in the formula $TmMn_{1-x}Co_xO_3$. This calculated P_{eff} is close to the experimental value. It is concluded from the P_{eff} value for x=0.5 that Co^{2+} must be HS. In Fig. 5, the x dependence of P_{eff} is also shown for Co^{3+}(HS) and Co^{3+}(LS). If the electronic state of Co^{3+} for x>0.5 is HS, P_{eff} increases with x. This contradicts the experimental results shown in Fig. 5. The values of P_{eff} agree qualitatively with calculations in which Co^{2+} and Co^{3+} are assumed to be in the HS and LS states, respectively.

For 0.5≤x≤0.7, both M_{FC} and M_{ZFC} increase ferromagnetically at $T_C \approx 58$ K with decreasing T. Since the ferromagnetic interaction is predominant for 0.5≤x≤0.7, this increase in magnetization is considered to be due to the canted magnetic transition of the Mn and Co ions, as reported for other rare-earth manganese oxides. The maximum values of M_{FC} are observed between 25 and 35 K. M_{FC} decreases with decreasing T and shows negative values below $T_{comp} \approx 13$ K for x=0.7. No ferromagnetic increase in magnetization is seen for x=0.8 and 0.9, although a small peak can be seen at about 44 K in M_{ZFC} for x=0.8. The discrepancy between M_{FC} and M_{ZFC} for x=0.8 and 0.9 is considered to be due to antiferromagnetic ordering or competition between ferromagnetic and antiferromagnetic interactions.

Another characteristic of the temperature dependence of M_{FC} below ~30 K for 0.5≤x≤0.7 is the rapid decrease with decreasing T. A similar decrease in M_{FC} is seen in other rare-earth manganese oxides.[18,20-23] Such a rapid decrease in M_{FC} indicates spin reversal phenomena related to rare-earth ions. The M-H curves for $TmMn_{0.5}Co_{0.5}O_3$ prepared by the solid-state

reaction method showed a large high-field magnetic susceptibility even below 20 K, which suggests that Tm^{3+} (J=6) is paramagnetic even at low temperatures. According to Cooke et al.,[21] the temperature dependence of M_{FC} can be fitted using the equation

$$M_{FC} = M_{Mn,Co} + \frac{C_{Tm}(H+H_{int})}{T-\Theta_W} \ , \qquad (4)$$

where $M_{Mn,Co}$ and H_{int} are the saturated moment and the internal field at the Tm sites due to the canted Mn-Co moment, respectively. C_{Tm} is the Curie constant for paramagnetic Tm^{3+} ions, Θ_W is the Weiss temperature, and H is the applied field, which is 250 Oe. The solid lines in Fig. 6 show that the temperature dependence of the magnetization below ~25 K can be well approximated using Eq. (4); the fitting parameters are listed in Table I. This successful model, which is based on a ferromagnetically ordered Mn-Co sublattice and a paramagnetic Tm sublattice, suggests that the negative internal field induced by the Mn-Co sublattice affects the Tm sublattice. It is considered that at low temperatures (below ~25 K), the Tm^{3+} spin is oriented in the direction opposite to H by H_{int}. Such spin inversion due to 3*d* transition metal elements and rare-earth elements seems to be common in perovskite-type oxides with the structure ABO_3, although the crystallographic reasons why H_{int} acts antiferromagnetically on the rare-earth element A are unclear.

4. Conclusion

From the plots of mass fraction vs x (insets of Figs. 2 and 3), the CP method was clearly demonstrated to be more suitable than the SSR method for $0.5<x\leq0.9$. Thus, we achieved the substitution of Mn through CP, and obtained almost a single orthorhombic phase for $0.5\leq x\leq0.9$ in $TmMn_{1-x}Co_xO_3$.

At $T > T_C \approx 58$ K, $TmMn_{1-x}Co_xO_3$, in which the Tm^{3+}, Mn^{4+}, Co^{2+}, and Co^{3+} ions are paramagnetic, is also paramagnetic. From the data on the unit cell volume and the effective moment, it is concluded that Co^{2+} has a high spin state (S=3/2) and that Co^{3+} in $TmMn_{1-x}Co_xO_3$ remains a low-spin-state ion (S=0). At $T = T_C$, a canted magnetic transition occurs as a result of the interaction between Mn and Co, and the magnetization increases ferromagnetically with decreasing T. Below the temperature at which M_{FC} is maximized, the interaction between Mn and Co ions induces a negative internal field H_{int} at the Tm sites. H_{int} reorients the Tm^{3+} spin in the direction opposite to the external field H. The total magnetization at low temperatures is explained on the basis of a two-sublattice model.

Acknowledgment

The authors would like to thank Prof. Hiroshi Isoda for his assistance with sample preparation.

References

1) T. Kimura, T. Goto, H. Shintani, K. Ishizuka, T. Arima, and Y. Tokura, Nature **426**, 55 (2003).
2) T. Goto, T. Kimura, G. Lawcs, A. P. Ramircz, and Y. Tokura, Phys. Rev. Lett. **92**, 257201 (2004).
3) J. Barier, D. Meier, K. Berggold, J. Hemberger, A. Balbashov, J. A. Mydosh, and T. Lorenz, Phys. Rev. B **73**, 100402(R) (2006).
4) J. R. Sahu, A. Ghosh, A. Sundaresan, and C. N. R. Rao, Mater. Res. Bull. **44**, 2123 (2009).
5) K. Asai, K. Fujiyoshi, N. Nishimori, Y. Satoh, Y. Kobayashi, and M. Mizoguchi, J. Phys. Soc. Jpn. **67**, 4218 (1998).
6) D. O'Flynn, C.V. Tomy, M. R. Lees, A. Daoud-Aladine, and G. Balakrishnan, Phys. Rev. B **83**, 174426 (2010).
7) V. L. Joseph Joly, P. A. Joy, and S. K. Date, Solid State Commun. **121**, 219 (2002).
8) J. Hemberger, F. Schrettle, A. Pimenov, P. Lunkenheimer, V. Yu. Ivanov, A. A. Mukhin, A. M. Balbashov, and A. Loidl, Phys. Rev. B **75**, 035118 (2007).
9) N. Iwata and K. Kohn, J. Phys. Soc. Jpn. **67**, 3318 (1998).
10) K. Yoshii and H. Abe, J. Solid State Chem. **165**, 131 (2002).
11) H. A. Salama and G. A. Stewart, J. Phys.: Condens. Matter **21**, 386001 (2009).
12) V. Yu Pomjakushin, M. Kenzelmann, A. Dönni, A. B. Harris, T. Nakajima, S. Mitsuda, M. Tachibana, L. Keller, J. Mesot, H. Kitazawa, and E. Takayama-Muromachi, New J. Phys. **11**, 043019 (2009).
13) H. A. Salama, G. A. Stewart, W. D. Hutchison, K. Nishimura, D. R. Scott, and H. StC. O'Neill, Solid State Commun. **150**, 289 (2010)
14) T. Tanaka, A. Kumagai, Y. Amakai, N. Momono, S. Murayama, and H. Takano, J. Korean Phys. Soc. **63**, 546 (2013).
15) C. Morilla-Santos, L. B. Arruda, C. A. Silva, and P. N. Lisboa-Filho, J. Electroceram. **27**, 215 (2011).
16) C. Moure, D. Gutierrez, J. Tartaj, and P. Duran, J. Eur. Ceram. Soc. **23**, 729 (2003).
17) F. Izumi and K. Momma, Solid State Phenom. **130**, 15 (2007).
18) O. Peña, A. B. Antunes, M. N. Baibich, P. N. Lisboa-Filho, V. Gil, and C. Moure, J. Magn. Magn. Mater. **312**, 78 (2007).

19) M. Ghiasi, M. U. Delgado-Jaime, A. Malekzadeh, R. P. Wang, P. S. Miedema, M. Beye, and F. M. F. de Groot, J. Phys. Chem. C **120**, 8167 (2016).
20) G. Demazeau, M. Pouchard, and P. Hagenmuller, C. R. Acad. Sci. Ser. C **277**, 109 (1973) [in French].
21) A. H. Cooke, D. M. Martin, and M. R. Wells, J. Phys. C: Solid State Phys. **7**, 3133 (1974).
22) J. Hemberger, S. Lobina, H. -A. Krug von Nidda, N. Tristan, V. Yu. Ivanov, A. A. Mukhin, A. M. Balbashov, and A. Loidl, Phys. Rev. B **70**, 024414 (2004).
23) Bibhuti B. Dash and S. Ravi, J. Magn. Magn. Mater. **429**, 281 (2017).

Figure Captions

Table I Fitting parameters for M_{FC} for x = 0.5, 0.6, and 0.7.

Fig. 1. (Color online) X-ray diffraction patterns for various $TmMn_{1-x}Co_xO_3$ samples. The XRD pattern for Tm_2O_3, which is considered an impurity, is shown at the top as a reference.

Fig. 2. (Color online) Lattice parameters and unit cell volume as functions of x. The open symbols were obtained from Ref. 19. The inset plots mass fraction vs x. All these values, except for those for x=0, were obtained from samples prepared by complex polymerization.

Fig. 3. (Color online) Temperature dependences of field-cooled (FC, filled symbols) and zero-field-cooled (ZFC, open symbols) magnetizations for $TmMn_{1-x}Co_xO_3$ for $0.0 \leq x \leq 0.4$, which were prepared by the solid-state reaction. The inset plots mass fraction vs x for samples prepared by the solid-state reaction.

Fig. 4. (Color online) Temperature dependences of field-cooled (FC, filled symbols) and zero-field-cooled (ZFC, open symbols) magnetizations for $TmMn_{1-x}Co_xO_3$ for $0.5 \leq x \leq 0.9$.

Fig. 5. (Color online) Effective paramagnetic moment P_{eff} and Weiss temperature Θ as functions of x for $TmMn_{1-x}Co_xO_3$. The filled (open) symbols are the experimental (calculated) P_{eff} data for the two-spin states of Co^{3+}.

Fig. 6. (Color online) Temperature dependence of M_{FC} for x = 0.5 to 0.7. The solid lines below 25 K are fits using Eq. (4).

Table I Fitting parameters for M_{FC} for x = 0.5, 0.6, and 0.7.

Co concentration x	$M_{Mn,Co}$ / emu g^{-1}	H_{int} / kOe	Θ_W / K
0.5	7.8	-4.0	-11
0.6	4.0	-3.0	-14
0.7	1.8	-2.1	-13

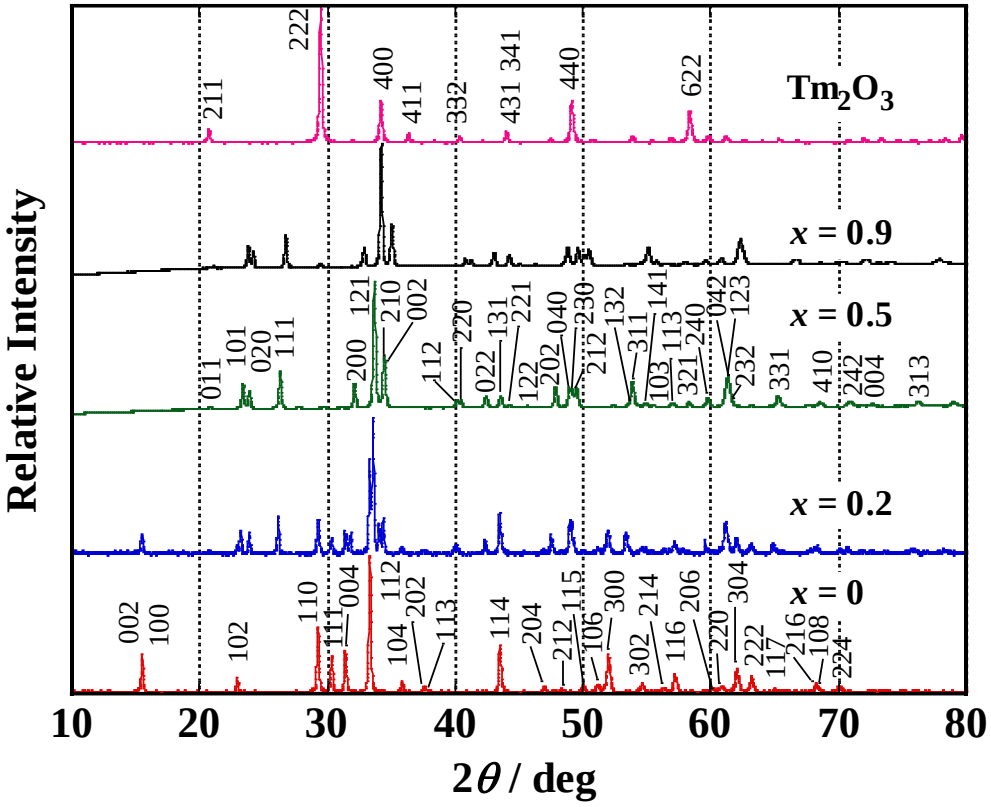

Fig. 1. (Color online) X-ray diffraction patterns for various $TmMn_{1-x}Co_xO_3$ samples. The XRD pattern for Tm_2O_3, which is considered an impurity, is shown at the top as a reference.

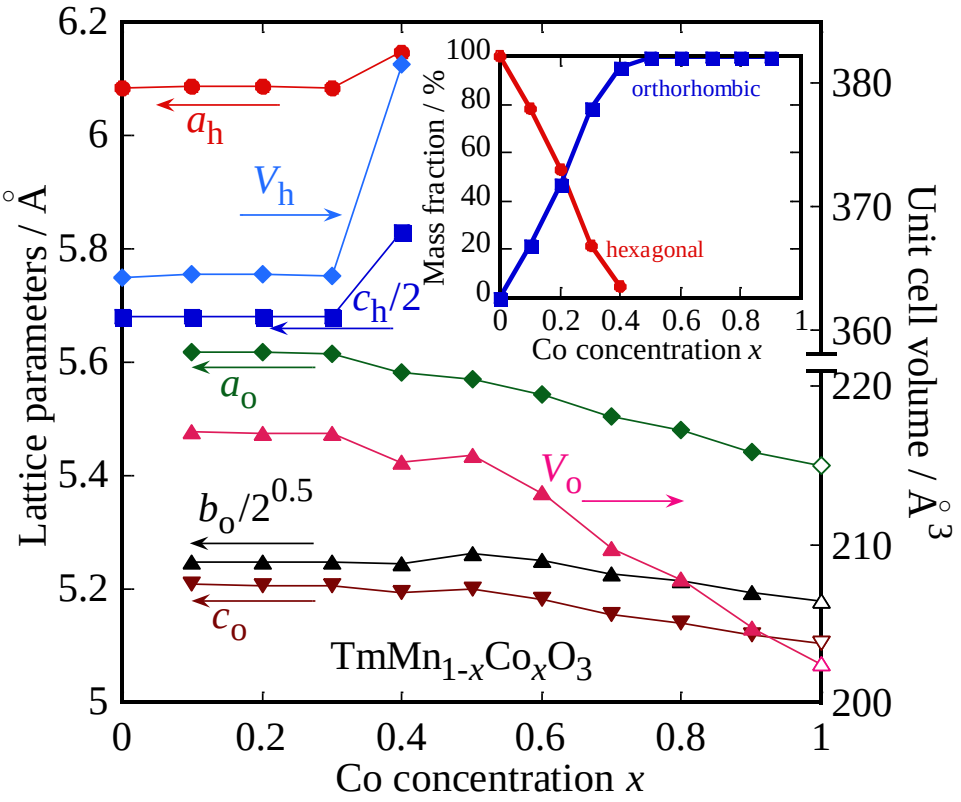

Fig. 2. (Color online) Lattice parameters and unit cell volume as functions of x. The open symbols were obtained from Ref. 19. The inset plots mass fraction vs x. All these values, except for those for x=0, were obtained from samples prepared by complex polymerization.

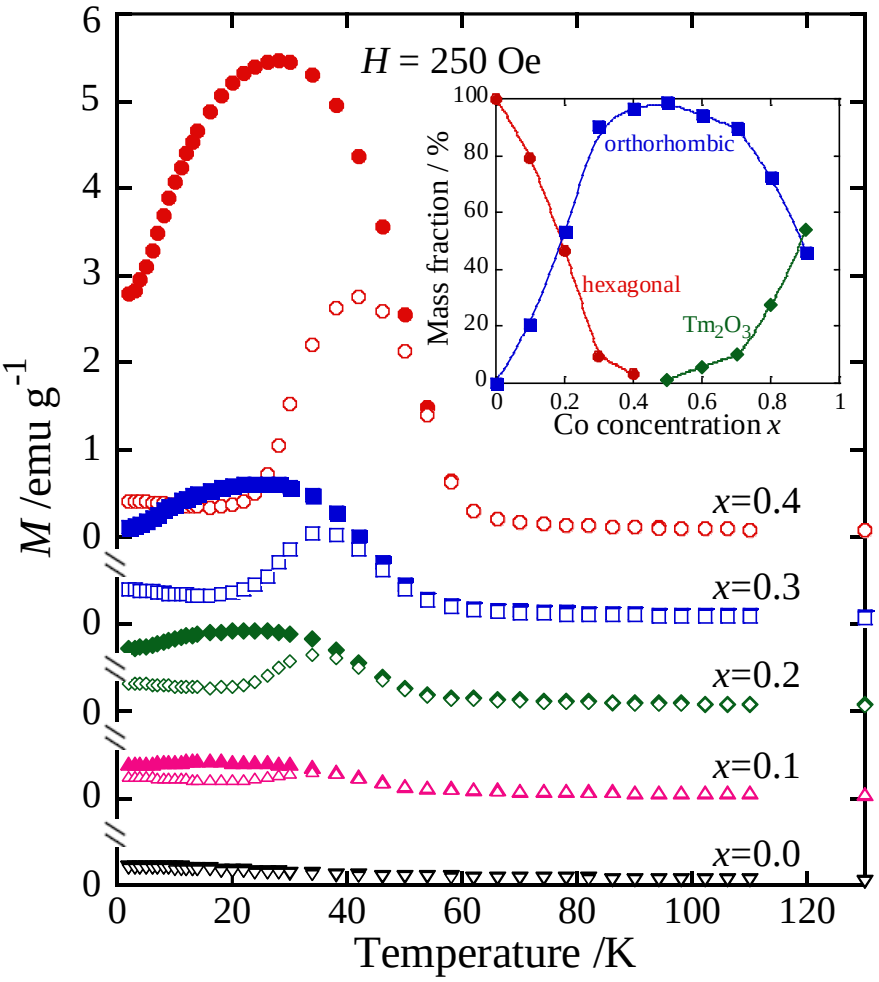

Fig. 3. (Color online) Temperature dependences of field-cooled (FC, filled symbols) and zero-field-cooled (ZFC, open symbols) magnetizations for $TmMn_{1-x}Co_xO_3$ for $0.0 \leq x \leq 0.4$ prepared by the solid-state reaction. The inset plots mass fraction vs x for samples prepared by the solid-state reaction.

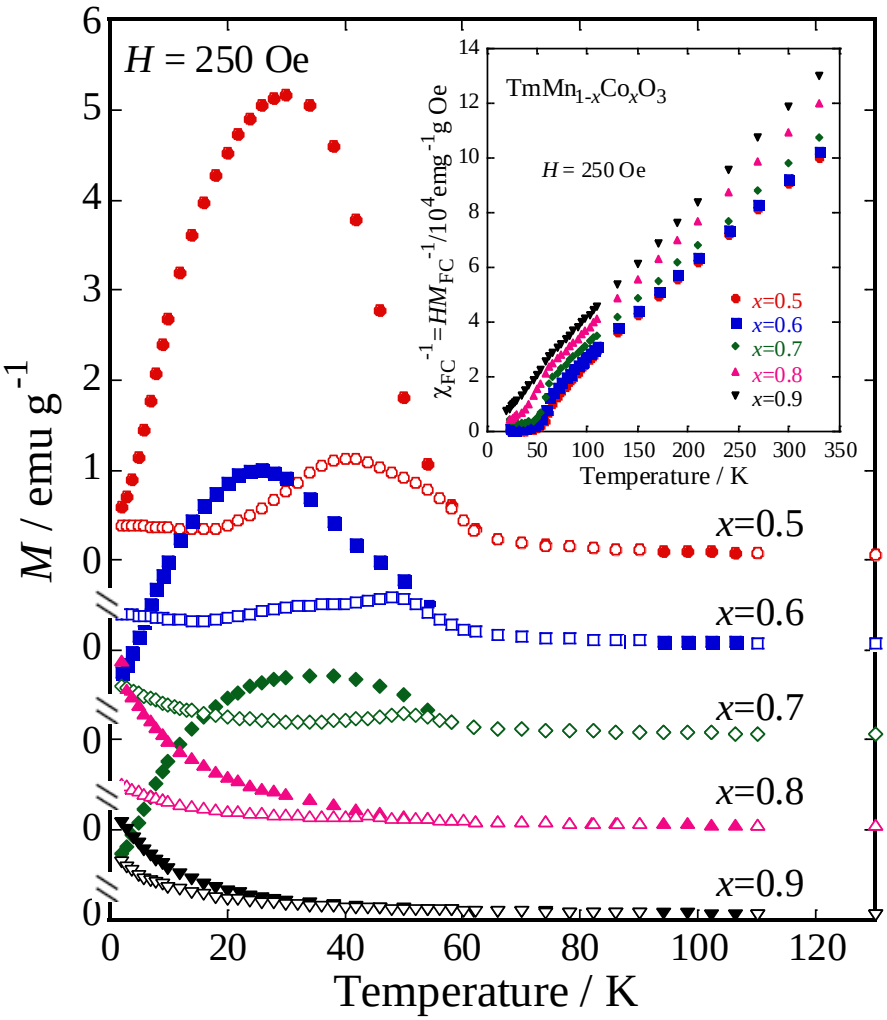

Fig. 4. (Color online) Temperature dependences of field-cooled (FC, filled symbols) and zero-field-cooled (ZFC, open symbols) magnetizations for $TmMn_{1-x}Co_xO_3$ for $0.5 \leq x \leq 0.9$.

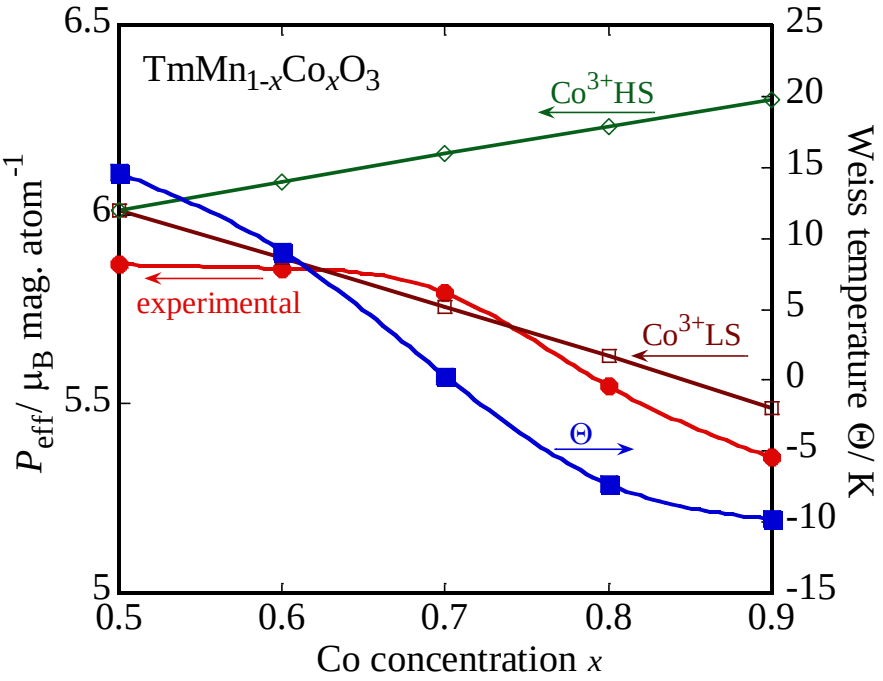

Fig. 5. (Color online) Effective paramagnetic moment P_{eff} and Weiss temperature Θ as functions of x for $TmMn_{1-x}Co_xO_3$. The filled (open) symbols are the experimental (calculated) P_{eff} data for the two spin states of Co^{3+}.

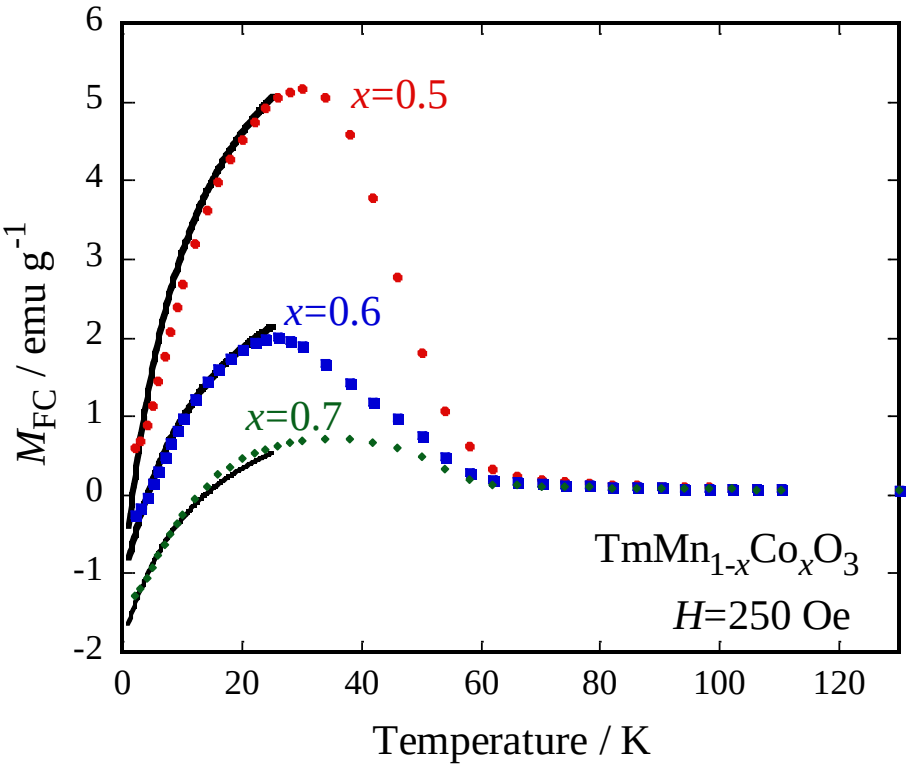

Fig. 6. (Color online) Temperature dependence of M_{FC} for x = 0.5 to 0.7. The solid lines below 25 K are fits obtained using Eq. (4).